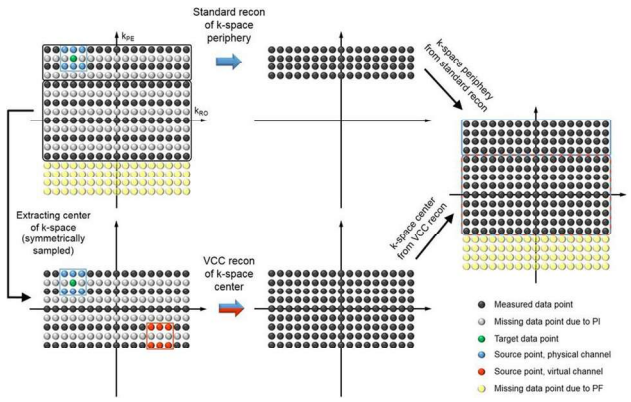

Combination of VCC and PF for in-plane acceleration. The central, symmetrically sampled region of k-space is reconstructed using the VCC signals, while the asymmetrically sampled periphery of k-space is reconstructed with standard GRAPPA. The two resulting datasets are combined to form a unified reconstructed k-space, which subsequently undergoes partial Fourier reconstruction. The concept is essentially the same for Slice-GRAPPA reconstruction of SMS accelerated data.

Results: Example SNR gain maps are shown in Fig. 2 for in-plane and SMS accelerations, for different PF factors. A general improvement of SNR is evident in both cases, increasing with higher PF factors. Locally, more than 100% SNR gain can be achieved.

The mean SNR gain within the brain is plotted in Fig. 3 for different PF factors. As expected, the benefit of VCC reconstruction decreases for stronger PF, but remains appreciable for the widely used 6/8 and 7/8 PF factors.

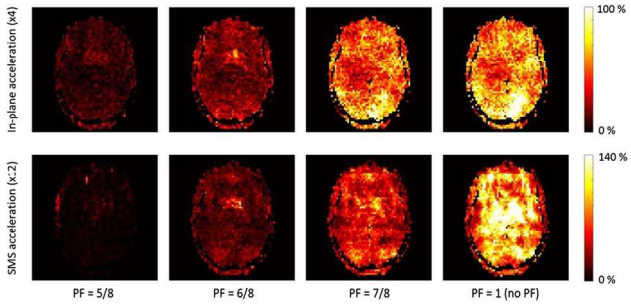

Spatial maps of SNR gain in the VCC reconstruction compared to the standard reconstruction, for an example slice of the brain. Results for in-plane acceleration (x4, upper row) and SMS acceleration (x12, bottom row) are displayed for different PF factors.

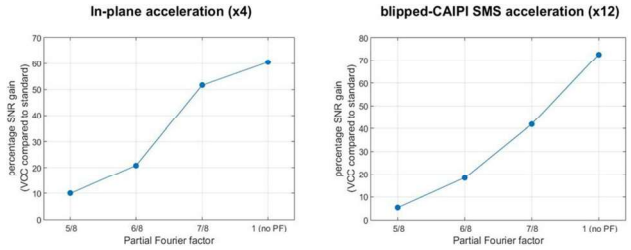

Mean SNR gain over the brain in VCC reconstruction compared to standard reconstruction for in-plane acceleration (left) and SMS acceleration (right), for different PF factors.

Discussion/Conclusion: We have shown that virtual conjugate coil reconstruction is applicable to partial Fourier parallel MRI, and can reduce noise relative to conventional reconstruction.

References:

[1] Blaimer, M., Gutberlet, M., Kellman, P., Breuer, F. A., Köstler, H., & Griswold, M. A. (2009). Virtual coil concept for improved parallel MRI employing conjugate symmetric signals. Magn Reson Med. 61(1), 93–102.

[2] Setsompop K, Gagoski BA, Polimeni JR, Witzel T, Wedeen VJ, Wald LL. Blipped-controlled aliasing in parallel imaging for simultaneous multi-slice echo planar imaging with reduced g factor penalty. Magn Reson Med. 2012;67(5):1210–1224.

[3] Griswold MA, Jakob PM, Heidemann RM, Nittka M, Jellus V, Wang J, Kiefer B, Haase A. Generalized autocalibrating partially parallel acquisitions (GRAPPA). Magn Reson Med. 2002;47(6):1202–1210.

[4] Haacke EM, Lindskogj ED, Lin W. A fast, iterative, partial-fourier technique capable of local phase recovery. J Magn Reson. 1991;92(1):126–145.

[5] Robson PM, Grant AK, Madhuranthakam AJ, Lattanzi R, Sodickson DK, McKenzie CA. Comprehensive quantification of signal-to-noise ratio and g-factor for image-based and k-space-based parallel imaging reconstructions. Magn Reson Med. 2008;60(4):895–907.

180

Model-based T1 Mapping with Sparsity Constraints Using Single-Shot Inversion-Recovery Radial FLASH

X. Wang[1], V. Roeloffs[1], J. Klosowski[1], Z. Tan[1], D. Voit[1], M. Uecker[2], J. Frahm[1]

[1]*Max Planck Institute for Biophysical Chemistry, NMR I, Goettingen/GERMANY,* [2]*Department of Diagnostic and Interventional Radiology, University Medical Center, GOETTINGEN/GERMANY*

Purpose/Introduction: To develop a model-based reconstruction technique for single-shot T1 mapping with high spatial resolution, accuracy and precision using an inversion-recovery (IR) FLASH acquisition with radial encoding.

Subjects and Methods: Ten subjects without known illness were recruited among the students of the local University. All measurements were performed on a human MRI system operating at 3T (Magnetom Prisma fit, Siemens Healthcare, Erlangen, Germany). The proposed model-based reconstruction jointly estimates all model parameters, i.e. the equilibrium magnetization, steady-state magnetization, 1/T1* and all coil sensitivities, directly from the data of a single-shot IR FLASH acquisition (4 s) with a small golden-angle radial trajectory, i.e.

$x = \text{argmin}_x \|F(x) - y\|_2^2 + \mu R(x)$ with $x = (M_{ss}, M_0, R1^*, c_1, \ldots, c_N)^T$.

The resulting nonlinear inverse problem is solved by the iteratively regularized Gauss–Newton method with joint sparsity constraints [1] on the parameter maps $(M_{ss}, M_0, R1^*)^T$ for performance improvement. Validations include both a numerical and experimental T1 phantom as well as in vivo studies of the human brain and liver. Abdominal measurements were performed during a brief breath hold.

Results: Figure 1 shows the determined M_0 maps, T1 maps and selected T1 line profiles obtained by NLINV reconstruction with subsequent pixel-wise fitting (top) as described in [2] and the proposed model-based reconstruction (bottom). Visual inspection and quantitative T1 line profiles demonstrate that the proposed method outperforms NLINV with respect to precision. Figure 2 compares corresponding M_0 and T1 maps of the human brain. In line with the simulation results, the latter method offers reduced noise and less

blurring. This comparison also holds true for applications to the human liver in Fig. 3. The magnified views clearly demonstrate the achievable improvement in spatial delineation of image details at high signal-to-noise ratio (e.g. vascular structures inside the liver).

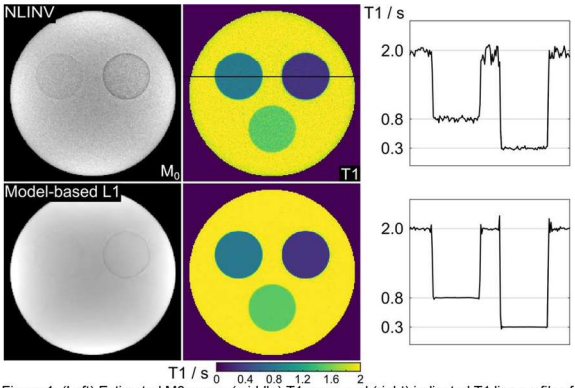

Figure 1. (Left) Estimated M0 maps, (middle) T1 maps and (right) indicated T1 line profiles for a numerical T1 phantom obtained by (top) NLINV reconstruction with pixel-wise fitting according to [2] and the proposed model-based reconstruction.

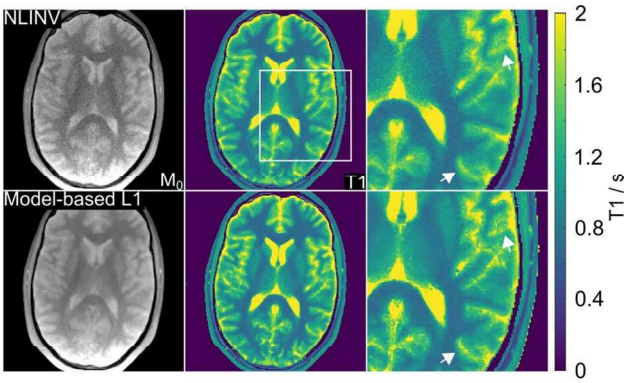

Figure 2. (Left column) Estimated M0 maps, (middle and right) T1 maps with magnified regions by (top) NLINV reconstruction with pixel-wise fitting according to [2] and (bottom) the proposed model-based reconstruction.

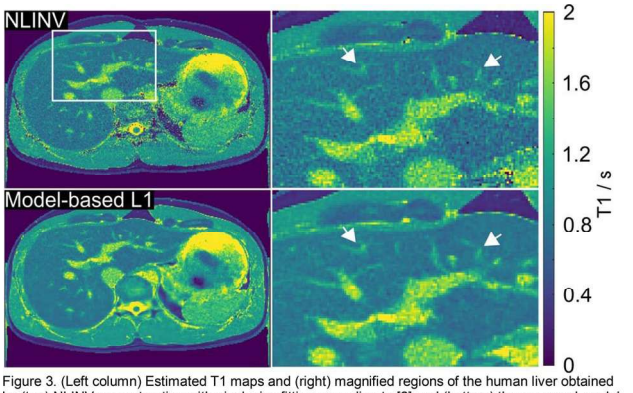

Figure 3. (Left column) Estimated T1 maps and (right) magnified regions of the human liver obtained by (top) NLINV reconstruction with pixel-wise fitting according to [2] and (bottom) the proposed model-based reconstruction.

Discussion/Conclusion: The proposed model-based reconstruction with sparsity constraints offers rapid and robust T1 mapping with high accuracy and precision. The method warrants accelerated computing and online implementation for extended clinical trials.

References:
[1] Wang X et al., *Magn Reson Med* (in press), doi: 10.1002/mrm.26726.
[2] Wang X et al., *Open Med Imaging J* (2015); 1–8.

181
Experimental study of bias in apparent exchange rate measurements

P. Ulloa, V. Methot, M.A. Koch
Institute of Medical Engineering, University of Luebeck, Luebeck/GERMANY

Purpose/Introduction: Double diffusion encoding (DDE)[1] MRI offers a new possibility to study microstructural characteristics non-invasively. In DDE, two independent pairs of diffusion gradients are applied between excitation and acquisition.[2] The technique has been proposed to study molecular exchange,[3] mapping the apparent exchange rate (AXR).[4–6] However, the same sequence can be used to retrieve microstructural information arising from restricted diffusion.[2,7] The coupling of these two effects may compromise AXR results, as suggested by a numerical simulation.[8] These calculations suggest that the restriction effect biases exchange measurements in samples comprising impermeable spheres with diameter >10 µm. The present work provides experimental confirmation of evidence for this phenomenon using a water-in-oil emulsion phantom.

Subjects and Methods: AXR[4] is measured by varying the time (τ_m) between two weighting periods (Fig. 1). The first diffusion weighting acts as a filter, while the second is used to calculate a τ_m-dependent apparent diffusion coefficient ($ADC'(\tau_m)$). Both weighting gradients are applied in the same direction. AXR is then calculated via $ADC'(\tau_m) = ADC \quad [1 - \sigma \quad \exp(-AXR\tau_m)]$ (ADC: "unfiltered" apparent diffusion coefficient, σ: filter efficiency).

DDE experiments were performed on a 3T whole-body MR system (Ingenia, Philips) using a phantom with impermeable pores (water-in-oil emulsion[9] with mean droplet diameter 15 µm according to optical microscopy). Experimental parameters are shown in Table 1 with Field-of-view = 196 × 196 × 5 mm^3. Two experiments were done to study the effect of different b values on AXR calculations.

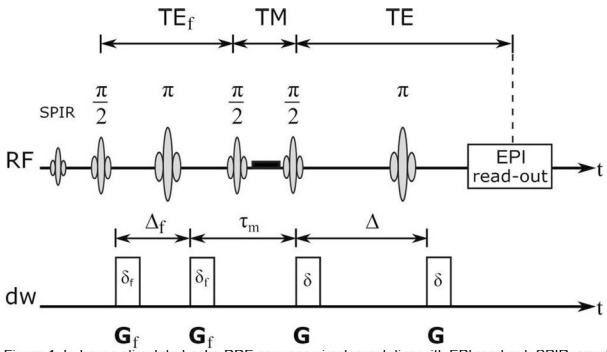

Figure 1: In-house stimulated-echo DDE sequence implementation with EPI read-out. SPIR: spectral presaturation with inversion recovery. Homospoil gradient pulse during longitudinal storage shown in solid black. τm = TM + ε is the time between the two innermost gradient pulses, where ε is fixed. All diffusion gradients (Gf and G) have equal duration and are trapezoidal in shape.